

Effect of the Normalizing Temperature on the Short-Time Creep of Martensitic 10Cr–3Co–3W–0.2Re Steel with a Low Nitrogen Content

I. S. Nikitin^{a, *} and A. E. Fedoseeva^{a, **}

^a Belgorod State National Research University, Belgorod, Russia

*e-mail: nikitin_i@bsu.edu.ru

**e-mail: fedoseeva@bsu.edu.ru

Received March 1, 2022; revised May 13, 2022; accepted June 1, 2022

Abstract—The short-time creep of martensitic 10Cr–3Co–3W–0.2Re (wt %) steel with a low nitrogen content subjected to normalizing at temperatures of 1050 and 1100°C and subsequent tempering at 770°C for 3 h is studied under the following creep conditions: the temperature is 650°C, and the applied stress is 200, 180, and 160 MPa. The time to failure is found to increase substantially in the steel at an increased normalizing temperature as a result of a longer transient creep stage and a decrease in the minimum creep rate under short-time creep conditions. An increase in the normalizing temperature from 1050 to 1100°C doubles the mean size of the initial austenite grain from 55 to 105 μm; in this case, the mean martensite lath width (about 300 nm) and the free dislocation density ($\sim 2 \times 10^{14} \text{ m}^{-2}$) are independent of the normalizing temperature. The increase in the initial austenite grain size as a result of the increase in the normalizing temperature is found to be accompanied by an increase in the fraction and extent of low-angle boundaries, which favors a decrease in the mean size of grain-boundary $M_{23}C_6$ carbide particles during tempering and a Laves phase during creep. Moreover, an increase in the normalizing temperature causes a decrease in the rate of coarsening of grain-boundary $M_{23}C_6$ particles, tungsten-rich particles, and carbonitride Nb(C,N) particles uniformly distributed over the matrix volume by a factor of 5 (for the first two particles) and 31, respectively.

Keywords: high-temperature martensitic steel, heat treatment, normalizing, creep, microstructure, secondary-phase particles, initial austenite grain, lath structure

DOI: 10.1134/S0036029522070102

INTRODUCTION

At the present time, both in Russia and abroad, the main tendency of developing thermal power on a coal fuel is related to the introduction in service of energy units operating of supercritical vapor parameters: the temperature is 600–620°C and the pressure is 24–33 MPa [1, 2]. Among the materials capable of holding these service conditions, there are high-chromium martensitic steels with a low nitrogen content and a high boron content [3–5]. A high chromium content provides good hardening characteristics, its solid-solution hardening and the participation of chromium in the formation of grain-boundary $M_{23}C_6$ -type carbide during tempering [1, 3, 5–7]. The addition of tungsten, molybdenum, and cobalt in steel composition increases the solid-solution hardening [4, 6, 7]; moreover, in the case of creep, tungsten and molybdenum form grain-boundary Laves phase particles [4–6]. Vanadium and niobium containing in the steel take part in the formation of M(C,N) carbonitrides, particles of which are homogeneously distributed over the matrix volume [3, 6, 8]. An increase in the boron

content in such steels decreases the rate of coarsening of $M_{23}C_6$ carbide particle during creep as a result of partial substitution of boron for carbon in them [3, 8]. As the nitrogen content in steel decreases, the formation of coarse BN particles is prevented on heating to the normalizing temperature, and the formation of coarse particles of Z-phase nitride replacing nanodispersed carbonitrides M(C,N) is prevented during creep [1, 9]. The high creep resistance of such steels is caused by long-term conservation of a tempered martensite lath structure with a high dislocation density in martensite lathes during creep, which is provided by the stabilization of such a structure with particles of $M_{23}C_6$ carbide, a Laves phase, and M(C,N) carbonitrides [3, 6–8].

Note that not only alloying of steel determines the structure characteristics (sizes of the initial austenite grains (IAG), packs, blocks, martensite laths, secondary-phase particles etc.), but also heat treatment conditions. In the literature, a great attention is given to the role of individual various alloying elements in the formation of the structure and properties upon creep

[1, 3–8], and there are a few works on the influence of heat treatment on the creep resistance of high-chromium steels [10–14]. In addition, up to now, there is no unambiguous answer to the question on the cause of increasing creep resistance of high-chromium steels as the normalizing temperature increases, since a change in the normalizing temperature influences not only the IAG size, but also a substructure, the volume fraction, and the dispersion of secondary-phase particles. In [14], we discussed the influence of the normalizing temperature on the creep resistance of 9Cr–1W–1Mo–V–Nb steel with the standard proportion of interstitial elements (0.1% C, 0.05% N, and 0.005% B).¹ An increase in the normalizing temperature was shown to increase the high-temperature strength of the steel due to the refinement of a martensitic structure with a simultaneous increase in precipitation hardening by M(C,N) carbonitride particles enriched in vanadium.

The studies of the influence of the normalizing temperature on the creep resistance of martensitic steels with a low nitrogen content, in which the main precipitation hardening is made by particles of $M_{23}C_6$ carbide and a Laves phase, are of particular interest. Unfortunately, the data obtained in [14] cannot be simply extrapolated to high-chromium steels with a low nitrogen content, since the fraction of M(C,N) carbonitrides in these steels are an order of magnitude lower and such particles do not give substantial hardening [7, 8].

In this work, we studied 10Cr–3Co–3W–0.2Re steel with a low nitrogen content and a high boron content, the peculiarity of which is high coarsening resistance of Laves phase and $M_{23}C_6$ carbide particles during creep as a result of added rhenium [15]. The aim of this work is to determine the influence of the normalizing temperature on the properties of the given martensitic steel during short-time creep at 650°C.

EXPERIMENTAL

The steel under study had the composition Fe_{base} –0.11C–0.03Si–0.14Mn–9.85Cr–3.2Co–0.13Mo–2.86W–0.23V–0.07Nb–0.03Ni–0.008B–0.002N–0.22Cu–0.17Re and was melted at the Institute für Eisenhüttenkunde (IEHK, Aachen, Germany) in a vacuum-induction furnace. After homogenization at 1150°C for 16 h, the steel was subjected to bilateral forging at 1150°C and heat treatment at two regimes: normalizing at temperatures of 1050 and 1100°C (holding for 1 h, cooling in air) followed by tempering at 770°C for 3 h (cooling in air). Thus, the heat treatment regimes differed in only the normalizing temperature.

Creep tests to fracture at 650°C and applied stresses of 200, 180, and 160 MPa (for brevity, creep at

650°C/200 MPa etc.) were carried out on planar samples with a cross section of $7 \times 3 \text{ mm}^2$ and a gage length of 25 mm using a lever-type ATS2330 testing machine, according to GOST 3248–81.

The IAG sizes were estimated by optical metallography (OM) of a metallographic section subjected to chemical etching in a 1% HF + 2% HNO₃ + 97% H₂O solution. Foils for transmission electron microscopy (TEM) and scanning electron microscopy (SEM) studies were thinned to thicknesses of 100–150 μm and subjected to electrolytic polishing in a 10% solution of perchloric acid in acetic acid at a voltage of 23 V and room temperature using a Struers TENUPO-5 device. Carbon replicas for TEM studies were prepared on a Quorum Q150R universal vacuum setup. TEM and SEM microstructural studies were carried out on a JEM JEOL-2100 microscope equipped with an energy-dispersive analysis attachment and on a Quanta 600 3D microscope equipped with an adapter for electron backscatter diffraction (EBSD) analysis, respectively. EBSD patterns were recorded from $300 \times 300 \text{ μm}$ areas at a scanning step of 0.1 μm. The martensite lath width was measured by the random intercept method taking into account all visible boundaries/subboundaries. Free dislocation density ρ in lathes was estimated as the number of points of emerging on the foil surface using TEM microphotographs and the Kernel coefficient (Kernel average misorientation) determined from EBSD patterns according to the expression [16]

$$\rho = 2\varphi/xb,$$

where φ is the Kernel average misorientation around each of the scanning points for the first coordination sphere (rad), x is the scanning step, and b is the Burgers vector.

The types of particles were determined by a combined method including a point measurement of the chemical composition and an analysis of electron diffraction by TEM of foils and carbon replicas, respectively. The equilibrium volume fraction of secondary-phase particles was determined using the ThermoCalc software.

RESULTS AND DISCUSSION

Short-Time Creep

Figure 1 shows the dependence of the time to failure on the applied stress for the 10Cr–3Co–3W–0.2Re steel with a low nitrogen content after heat treatment under various conditions. An increase in the normalizing temperature is seen to substantially increase the time to failure by ~2 and ~7 times at applied stresses 200 and 160 MPa, respectively. Time to failure τ_r can be expressed as the dependence on applied stress σ as follows [10]:

$$\tau_r = A\sigma^{-m},$$

¹ From here on, the element content is given in wt %.

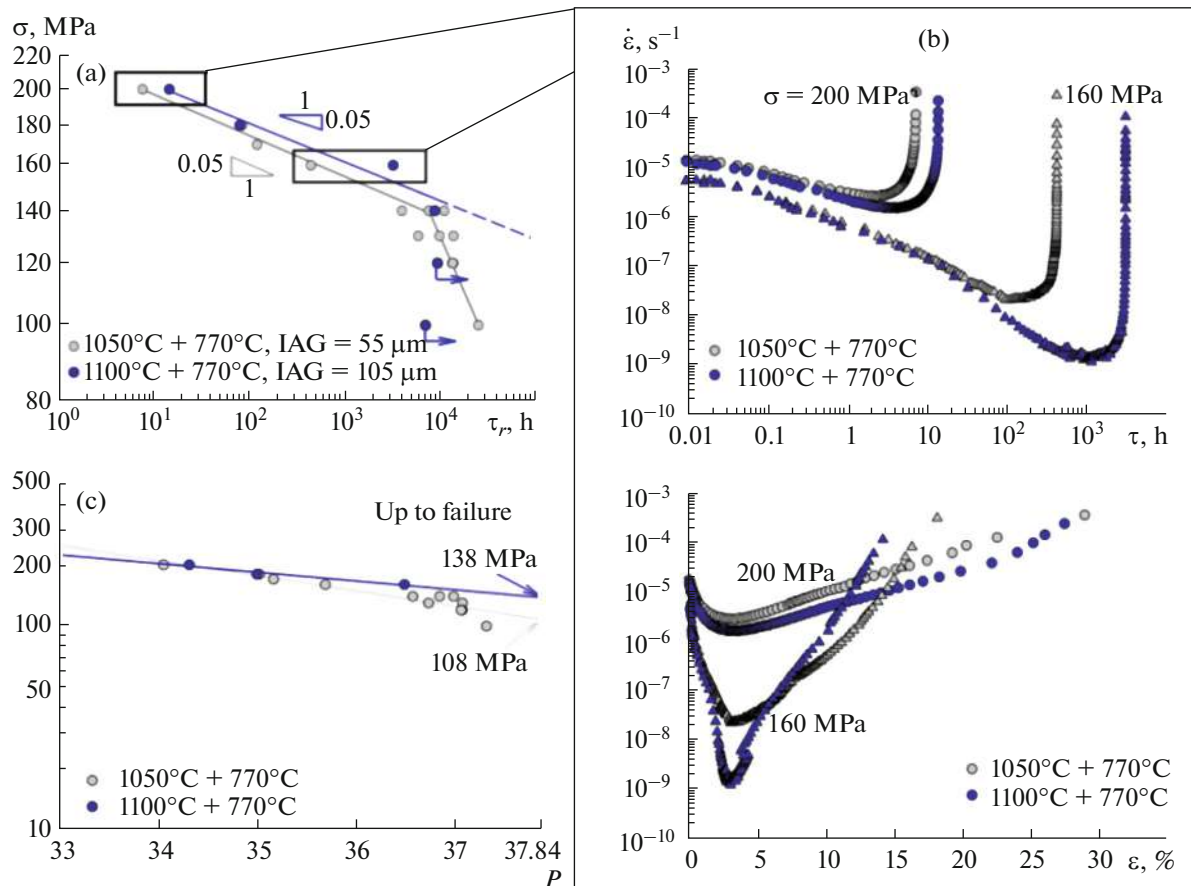


Fig. 1. (a) Long-term strength curve (τ_r is the time to failure), (b) strain rate $\dot{\epsilon}$ vs. time τ and creep strain ϵ for applied stresses of 200 and 160 MPa, and (c) Larson–Miller parameter P vs. the applied stress for the steel at 650°C.

where A is a constant and m is the stress constant (MPa/h).

In the region of short-time creep, the stress constant is 0.05 MPa/h for the steel samples subjected to normalizing at 1050 and 1100°C (Fig. 1a). The obtained stress constant agrees well with the values obtained for high-chromium steels, such as P92 and P911, which are within the range from 0.05 to 0.14 MPa under dislocation creep conditions [5, 10–12, 14].

To reveal the factors of increasing the time to failure at applied stresses of 200 and 160 MPa for the samples subjected to normalizing at 1100°C, we compared the curves of the dependence of strain rate $\dot{\epsilon}$ on time τ and strain ϵ (Fig. 1b). Table 1 gives the parameters obtained from the creep curves of the steel at applied stresses of 200 and 160 MPa. The main differences in the behavior of the samples subjected to normalizing at various temperatures consist in the transient creep stage time and the minimum creep rate $\dot{\epsilon}_{\min}$. For example, for the samples subjected to normalizing at 1100°C, the minimum strain rates at applied stresses 200 and 160 MPa decrease by factors of ~ 2 and ~ 18 , respectively, and the times required to attain the minimum strain rates increase by factors ~ 2 and ~ 11 ,

respectively (Table 1). In this case, the strains at which the minimum creep rates are reached, are 3.4–3.6% and 3.0–3.1% at applied stresses 200 and 160 MPa, respectively, independently of the normalizing temperature (Fig. 1b). The high strain rate (about 3%) at which the minimum creep rate is reached is typical of chromium steels (10% Cr) with a low nitrogen content [3, 5, 8, 15] as compared to steels containing 0.05% nitrogen, in which the minimum creep rate takes place at a strain of $\sim 1\%$ [11, 14]. As the applied stress decreases from 200 to 160 MPa, the difference between the strains to failure for the samples subjected to normalizing at 1050 and 1100°C increases from 5 to 20% (Fig. 1b, Table 1).

We preliminarily estimated the long-term ultimate strength using the empiric Larson–Miller dependence [17]

$$P = T(\log \tau_r + 36) \times 10^{-3},$$

where P is the Larson–Miller parameter, T is the creep temperature (K), and τ_r is the time to failure (h).

Figure 1c shows the dependence of the applied stress on the Larson–Miller parameter for the 10Cr–3Co–3W–0.2Re steel after normalizing at tempera-

Table 1. Effect of normalizing temperature t_{norm} on the creep parameters of the steel at 650°C and applied stresses of (numerator) 200 MPa and (denominator) 160 MPa

Parameter	Parameter at t_{norm} , °C	
	1050	1100
Time to failure τ_r , h	7.6/440.5	14.5/3207.6
Strain to failure, %	28.9/18.8	27.4/14.8
Minimum creep rate $\dot{\epsilon}_{\text{min}}$, s^{-1}	$2.75 \times 10^{-6}/2.20 \times 10^{-8}$	$1.60 \times 10^{-6}/1.23 \times 10^{-9}$
Time to reach $\dot{\epsilon}_{\text{min}}$, h	2.6/110.3	4.4/1198.7
Strain at $\dot{\epsilon}_{\text{min}}$, %	3.44/3.12	3.58/3.04

tures 1050 and 1100°C followed by tempering at 770°C. The extrapolation was carried out for a holding time of 10^5 h (~11.6 years). For this steel normalized at 1100°C, the preliminary long-term ultimate strength for 10^5 h at temperature of 650°C is 138 MPa, which is 28% higher than that after normalizing at 1050°C.

Initial Structure of the Steel after Heat Treatment under Various Conditions

Figures 2a and 2b show OM results for the 10Cr–3Co–3W–0.2Re steel. After normalizing at both tem-

peratures, the steel structures are 100% martensite and δ -ferrite grains were not detected. An increase in the normalizing temperature from 1050 to 1100°C leads to doubling the mean IAG size, from 55 to 105 μm . The increase in the austenite grain size is, first, due to the dissolution of Nb(C,N) carbonitride particles. For example, an increase in the temperature from 1050 to 1100°C leads to a decrease in the volume fraction of Nb(C,N) carbonitride particles from 0.05 to 0.03%, according to the mathematical modeling using the Thermo-Calc software. A decrease in the retarding Zener forces from homogeneously distributed

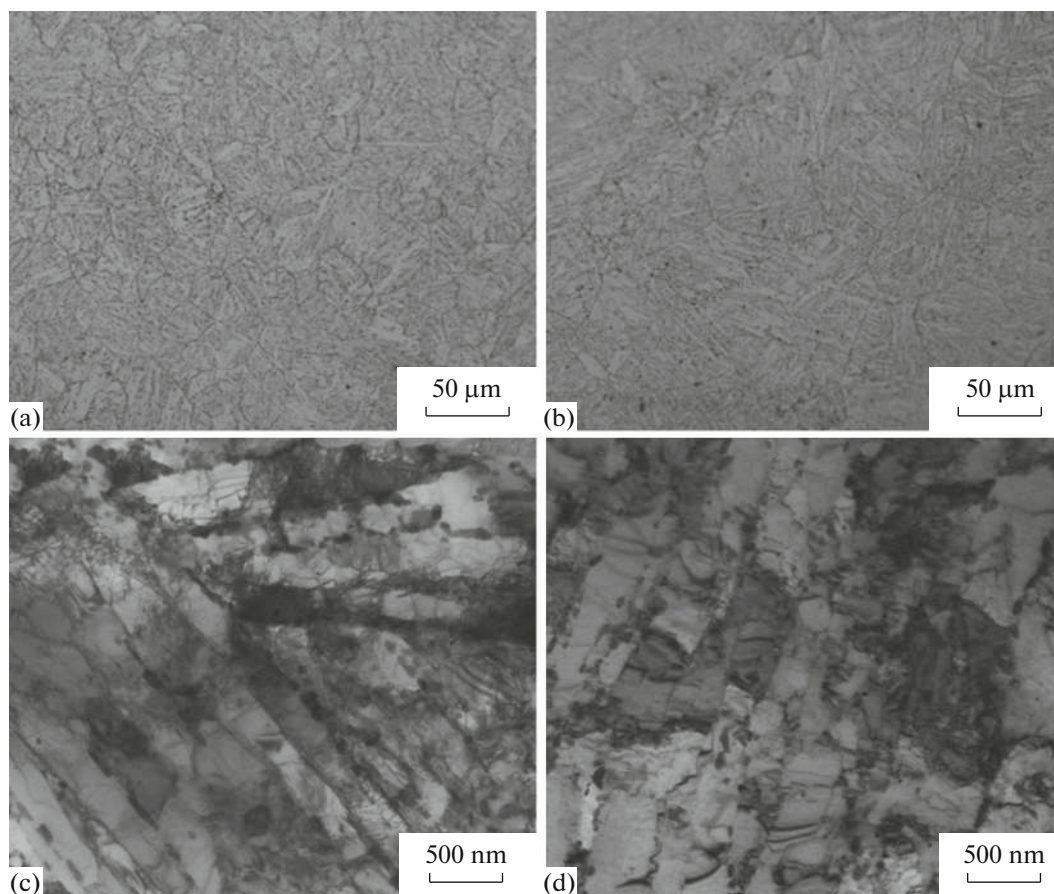
**Fig. 2.** Microstructures of the steel normalized at (a, c) 1050°C and (b, d) 1100°C and then tempered at 770°C for 3 h: (a, b) MO and (c, d) TEM.

Table 2. Effect of the normalizing temperature on the structure and secondary-phase particles in the steel after normalizing at various temperatures and tempering at 770°C

Parameter	Parameter at t_{norm} , °C	
	1050	1100
OM and TEM data:		
IAG average size	55	105
average lath width, nm	293	296
dislocation density, $\times 10^{14} \text{ m}^{-2}$	1.98	2.00
average particle size, nm: M_{23}C_6	67	59
Nb(C,N)	37	34
M_6C	28	44
particle density along LABs* of martensitic laths, μm^{-1}	4.73	6.11
Volume fraction of particles**, %: M_{23}C_6	2.21	2.21
Nb(C,N)	0.081	0.079
EBSD data:		
fraction of LABs, %	51.3	56.7
fraction of HAB***, %	48.7	43.3
LAB/HAB ratio	1.05	1.31
total length, cm: LAB	5.52	5.55
HAB	5.10	5.48
boundaries	10.62	11.03
Average KAM ϕ , deg	0.56	0.59
Dislocation density, $\times 10^{14} \text{ m}^{-2}$	3.94	4.13

* Low-angle boundaries.

** According to the Thermo-Calc mathematical simulation.

*** High-angle boundaries.

Nb(C,N) carbonitrides causes an increase in the IAG size at a higher temperature [18].

SEM showed that a tempered troostite structure forms in the steel irrespective of the normalizing temperature (Figs. 2c, 2d). The parameters of the structure and secondary-phase particles after normalizing at 1050 and 1100°C followed by the tempering at 770°C are given in Table 2. The change in the normalizing temperature did not lead to a change in the martensite lath width and the free dislocation density. After treatment according to both regimes, the martensite lath width was ~ 300 nm and the free dislocation density was $\sim 2 \times 10^{14} \text{ m}^{-2}$ (Table 2). Figure 3 shows micrographs of secondary-phase particles revealed after both types of heat treatment in the case of normalizing at 1100°C followed by tempering at 770°C.

The dominant secondary phase is the M_{23}C_6 carbide with the mean chemical composition 50% Cr, 20–25% Fe, and 25–30% W (Fig. 3a). The volume fraction of this phase is 2.21% independent of the normalizing temperature (Table 2). After both types of treatment, M_{23}C_6 carbide particles were revealed

along the boundaries of IAG, packs, blocks, and martensite laths. An increase in the normalizing temperature from 1050 to 1100°C led to a decrease in the mean size of M_{23}C_6 carbide particles from 67 to 59 nm, which was accompanied by an increase in the density of these particles along the low-angle boundaries (LABs) of martensite laths by 29% (Table 2). Most of the M_{23}C_6 carbide particles arranged along the LABs of martensite laths have orientation relationships with the martensite matrix (Fig. 3c), which demonstrates partial coherence or semicoherence of M_{23}C_6 carbide particle/matrix boundaries [15]. In addition, after normalizing of both types, the steel structure was found to have Nb(C,N) carbonitride particles containing 70–74% Nb and M_6C carbide enriched in tungsten (69% W) [19]. Figures 3d–3f and 3g–3i show dark-field (DF) and bright-field (BF) images of Nb(C,N) and M_6C particles, respectively, in a steel sample after normalizing at 1100°C followed by tempering at 770°C. The mean sizes of Nb(C,N) particles in the samples subjected to normalizing at 1050 and 1100°C are 37 and 34 nm, respectively; in this case, the volume fractions of these particles after various heat

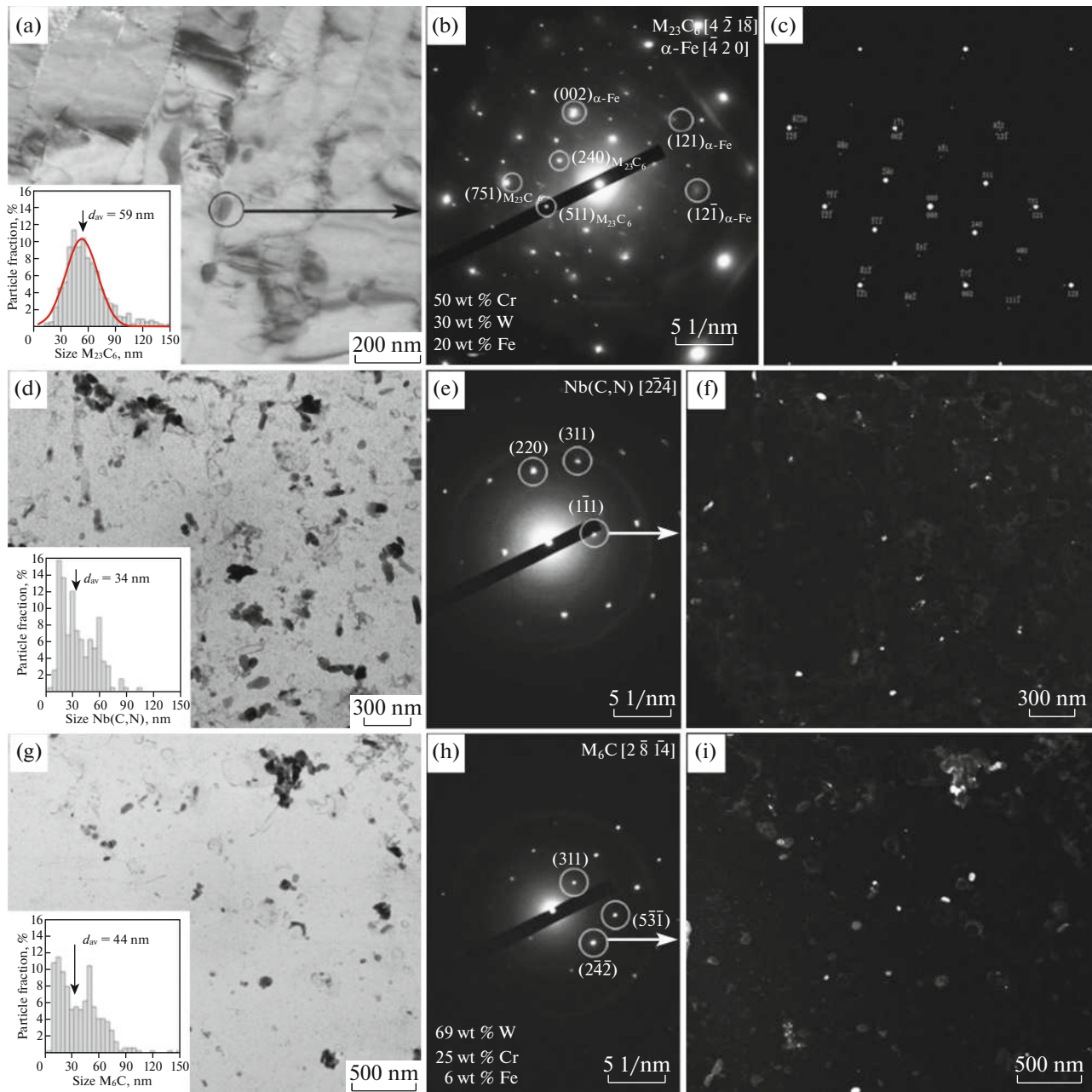


Fig. 3. Images of secondary-phase particles in the steel after normalizing at 1100°C and subsequent tempering at 770°C: (a) image of carbide $M_{23}C_6$ in a martensite matrix combined with (b) diffraction pattern from the carbide $M_{23}C_6$ particle/matrix interface, (c) orientation relationship obtained with the Crystal-studio program; (d) bright-field (BF) image of particles on a carbon replica with (e) diffraction pattern from carbonitride Nb(C,N) particles and (f) the corresponding dark-field (DF) image taken with the $(1\bar{1}1)_{Nb(C,N)}$ reflection; (g) BF image of particles on a carbon replica with (h) diffraction pattern from carbide M_6C particle and (i) corresponding DF-image taken with the $(2\bar{4}2)_{M_6C}$ reflection.

treatment are almost the same (Table 2). The mean sizes of M_6C particles in the samples subjected to normalizing at 1050 and 1100°C are 28 and 44 nm, respectively (Table 2).

Thus, the causes of increasing the creep resistance of the steels with 9–10% Cr and various nitrogen contents are ambiguous. In the low-nitrogen steels, the

increase in the creep resistance during short-time tests cannot be related to a refinement of the martensitic structure or to an increase in the contribution of precipitation hardening from the precipitation of $M(C,N)$ carbonitride, as was found in P911 steel [14]. A more detailed study of the influence of the state of LABs on the distribution of secondary-phase particles was car-

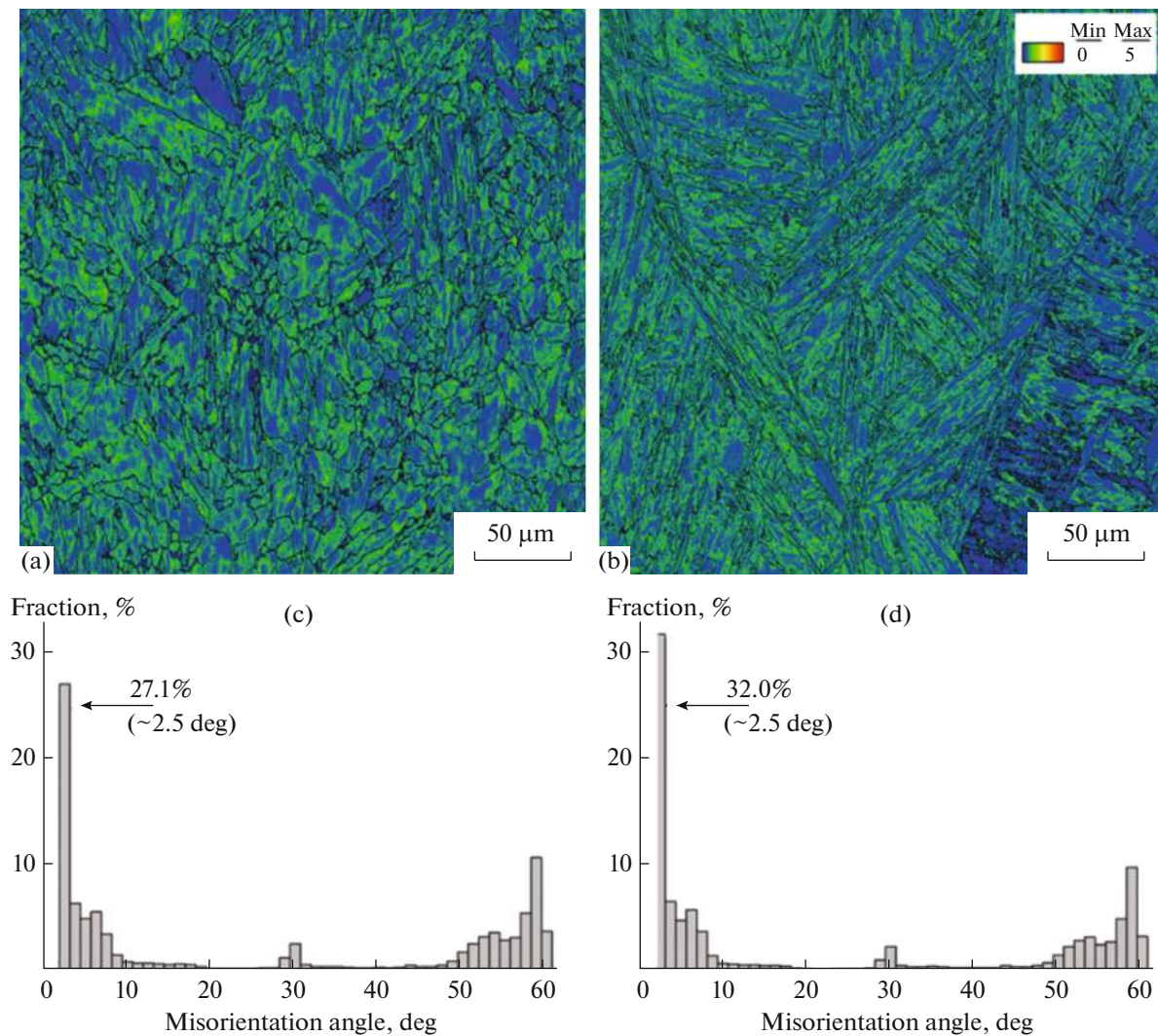


Fig. 4. Distribution maps of (a, b) Kernel coefficient and (c, d) misorientation angles for the steel normalized at (a, c) 1050°C and (b, d) 1100°C and then tempered at 770°C.

ried out by EBSD analysis. We constructed lattice distortion distribution maps in the form of Kernel coefficient distributions and misorientation angle distribution histograms for the steel after normalizing at 1050 and 1100°C followed by tempering at 770°C (Fig. 4). The data obtained from the EBSD maps are given in Table 2.

According to the data shown in Figs. 4a and 4b, the distribution of the Kernel coefficient is inhomogeneous with a scatter of 0° – 2° . The mean Kernel coefficients for the steel normalized at 1050 and 1100°C are 0.56° and 0.59° , respectively (Table 2); i.e., the values are close. From the data on the distribution of misorientation angles, it follows that an increase in the normalizing temperature from 1050 to 1100°C leads to an increase in the fraction of LABs from 51.3 to 56.7% (Table 2). Note substantial differences for boundaries ($\sim 2.5^{\circ}$), which are 27.1 and 32.0% for the samples sub-

jected to normalizing at 1050 and 1100°C, respectively (Figs. 4c, 4d). According to [20, 21], an angle of $\sim 2.5^{\circ}$ corresponds to the mean misorientation of martensite lath boundaries. The dislocation densities estimated by TEM and EBSD have close values and are about $(2\text{--}4) \times 10^{14} \text{ m}^{-2}$ irrespective of the normalizing temperature (Table 2). Note that the increase in the fraction of LABs and their total length is accompanied by a decrease in the mean size of grain-boundary particles and an increase in their density along the LABs of martensite laths. As was shown in [22], the distribution of $M_{23}C_6$ carbide particles along the LABs of martensite laths causes the nucleation of grain-boundary Laves phase particles, the precipitation of which determines the behavior of steel at the transient creep stage. For example, an increase in the time to failure of the steel subjected to normalizing at 1100°C is most

Table 3. Structural parameters of the steel normalized at (numerator) 1050°C and (denominator) 1100°C and then tempered at 770°C after creep tests at 650°C and applied stresses of 200 and 160 MPa

Parameter	Parameter at stress, MPa	
	200	160
Time to failure τ_r , h	8/15	440/3207
Average lath width, nm	500/490	573/561
Dislocation density, $\times 10^{-14} \text{ m}^{-2}$	0.7/0.7	1.03/0.36
Average particle size, nm: $M_{23}C_6$	75/63	81/70
Nb(C,N)	35/37	50/41
W-rich	60/23	106/100
Volume fraction, %; $M_{23}C_6$	2.21/2.21	2.21/2.21
M(C,N)	0.081/0.079	0.081/0.079
$(\text{Fe,Cr})_2\text{W}$	—/—	1.84/1.84

* According to the Thermo-Calc mathematical simulation.

likely to be related to the structural changes occurring during creep.

Structural Changes during Short-Time Creep

The increase in the time to failure of the samples subjected to normalizing at 1100°C in short-time creep tests at stresses of 200 and 160 MPa (Fig. 1b) is due to substantial hardening at the transient creep stage, which leads to an increase in the duration of this stage simultaneously with a decrease in the minimum strain rate. The substantial hardening at the transient creep stage is usually associated with the precipitation of fine Laves phase particles along the boundaries of IAGs, blocks, packs, and martensite laths [1, 3, 6, 8, 10, 12, 15, 19]. M_6C carbides are the nucleation centers for precipitating Laves phase particles in steels with 9–10% Cr and 3% W and/or in steels with 10% Cr and low nitrogen content [19, 22]. The significant difference between the samples normalized at various temperatures, after a creep test at 650°C and a stress of 200 MPa was related to the place of M_6C carbide nucleation. In the steel normalized at 1050°C, M_6C carbides were found to nucleate at $M_{23}C_6$ /matrix boundaries and also individually at martensite lath boundaries; in this case, the size of the particles located along lath boundaries is larger than those on $M_{23}C_6$ carbides by a factor of two [19]. In contrast, in the steel normalized at 1100°C, M_6C carbides are only observed along $M_{23}C_6$ particle/matrix boundaries, and the average size of such particles is 23 nm (Table 3). Laves phase particles precipitate along the boundaries at a longer creep time under conditions 650°C/180 MPa after both types of heat treatment. After creep test until failure under conditions 650°C/160 MPa, the average size of the Laves phase particles was ~100 nm after both types of heat treatment. The chemical compositions of the Laves phase in the samples normalized at

both the temperatures are close, 66% W, 18% Fe, and 16% Cr, which is typical of the Laves phase particles in steels with 9–10% Cr [1, 3–5, 10, 12, 15, 19, 22]. The volume fractions of Laves phase particles are the same after both normalizing temperatures; it is 1.84% according to the calculations in the Thermo-Calc software.

At the same time, the structure stability expressed as a widening of martensite laths and a decrease in the dislocation density also determines the time to failure of creep samples [3, 6, 10]. The structure stability, at least in the short-time creep region, is dependent on the stability of grain-boundary particles and the M(C,N) carbonitride particles distributed homogeneously over the matrix volume. Table 3 gives the structural parameters of the steels subjected to heat treatment under various conditions after creep tests at 650°C/200 MPa and 650°C/160 MPa. For short-time creep under conditions 650°C/160 MPa, it was revealed that the lath widths increase to 573 nm and 561 nm after normalizing at 1050 and 1100°C, respectively; the free dislocation density decreases more intensely during creep after normalizing at 1100°C. To describe the growth of the structural elements, the following relationship in terms of the Lifshitz–Slyozov–Wagner (4) theory is valid [23, 24]:

$$d^n - d_0^n = K_{\text{growth}}(\tau - t_0),$$

where d is the average particle size at current time τ (μm), d_0 is the initial particle size at time t_0 , K_{growth} is the growth rate constant ($\mu\text{m}^n \text{ s}^{-1}$), τ is time, and n is the coefficient depending on the growth mechanism ($n = 3$ for volume diffusion, $n = 4$ for grain-boundary diffusion, $n = 5$ for pipe diffusion). Figure 5 shows the time dependences of the martensite lath size and the secondary-phase particle size during creep for estimating the growth rate of structural elements.

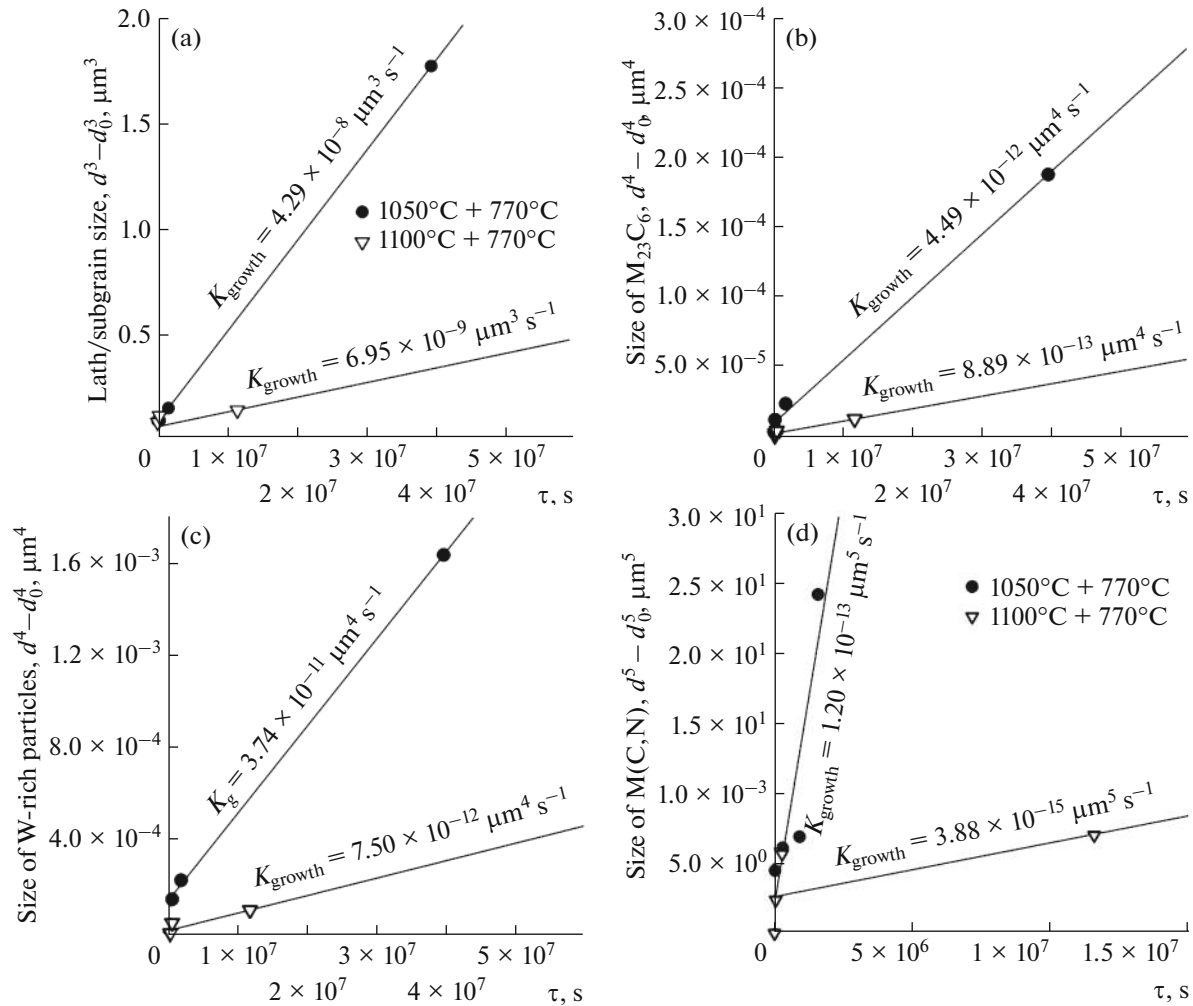


Fig. 5. Time changes in the sizes of various structural elements during creep: (a) martensite laths (subgrains), (b) carbide M_{23}C_6 particles, (c) W-rich particles (M_6C , Laves phase), and (d) carbonitride $\text{M}(\text{C},\text{N})$ particles.

In the steel subjected to normalizing at 1100°C , the martensite laths are widened at a growth rate $6.95 \times 10^{-9} \mu\text{m}^3 \text{s}^{-1}$ provided that the growth mechanism of martensite laths is volume diffusion (Fig. 5a). This growth rate constant of martensite laths is an order of magnitude lower than that observed in the steel samples subjected to normalizing at 1050°C (Fig. 5a). Note that the low growth rate of martensite laths correlates with the decrease in the growth rate of all secondary-phase particles in the steel samples subjected to normalizing at 1100°C (Figs. 5b–5d). For example, the growth rate of M_{23}C_6 carbide particles and the particles enriched in tungsten (M_6C , Laves phase) in the steel samples subjected to normalizing at 1100°C is five times lower than that in the steel samples subjected to normalizing at 1050°C provided that the growth mechanism of these particles is grain-boundary diffusion. Such a substantial decrease in the growth rate of grain-boundary secondary-phase particles is likely to be due to a low particle–matrix inter-

face energy [15]. Most of the M_{23}C_6 carbide particles do not lose orientation relationships with the matrix, which can demonstrate that partial coherence or semi-coherence of the boundaries is retained [15]. The large extent of the LABs of martensite laths in the steel samples subjected to normalizing at 1100°C ensures more potential places for the formation of Laves phase nuclei, which decreases the initial particle size and increases the particle density along lath LABs.

The significant decrease in the growth rate of the Laves phase increases the contribution of the precipitation hardening from these particles to the total strength at the transient creep stage. The precipitation of fine Laves phase particles upon creep after normalizing at 1100°C is assumed to be an effective mechanism of increasing the creep resistance in the steel under study. Significant hardening leading to an increase in the transient stage time with a significant decrease in the minimum strain rate was also observed in [25, 26], when an increase in the tungsten content

in steel led to an increase in the transient creep stage time, a decrease in the minimum strain rate, and an increase in the total time to failure. For example, for the creep at 600°C/137 MPa, the minimum strain rate decreased from 5.56×10^{-7} to $2.78 \times 10^{-9} \text{ s}^{-1}$ as the tungsten content in the steel with 9% Cr and 0.1% C is changed from 1 to 4% [26]. In [25, 26], the contribution of Laves phase particles to the strength of steel increased as a result of increasing in the fraction of these particles. In this work, the increase in the creep resistance is associated with the formation of finer Laves phase particles at the same their volume fraction.

A similar situation is also observed for Nb(C,N) carbonitride. The growth rate of Nb(C,N) carbonitride particles in the steel samples normalized at 1100°C is lower than that in the steel samples normalized at 1050°C by a factor of 31. In total, these two factors stabilize the lath structure of tempered troostite during a longer time in the creep process, which increases the transient creep stage time and, as a result, the time to failure.

CONCLUSIONS

(1) An increase in the normalizing temperature from 1050 to 1100°C in low-nitrogen 10% Cr–3% Co–3% W–0.2% Re steel led to an increase in the time to failure by factors of ~2 and ~7 under the creep conditions 650°C/200 MPa and 650°C/160 MPa (numerator, the creep test temperature; denominator, the applied stress).

(2) The increase in the time to failure was accompanied by an increase in the transient creep stage time and a decrease in the minimum creep rate under both creep conditions.

(3) An increase in the normalizing temperature from 1050 to 1100°C ensured doubling the average IAG size, which was accompanied by an increase in the fraction and the total extent of the low-angle boundaries of martensite laths. The latter led to the refinement of $M_{23}C_6$ carbide particles during tempering and Laves phase particles during creep, which was accompanied by an increase in the numerical particle density along the boundaries.

(4) The substantial increase in the time to failure of the samples normalized at 1100°C is related to the precipitation of fine Laves-phase particles and to the retardation of the growth of $M_{23}C_6$ carbide and Nb(C,N) carbonitrides by factors of 5 and 31, respectively.

FUNDING

The microstructure and mechanical property studies were supported by the Russian Foundation for Basic Research, project no. 20-33-90117, and the phase composition simulation was supported by a grant of the President of

the Russian Federation for supporting young scientists, Candidates of Sciences, project no. 075-15-2021-336.

The work was carried out using equipment of the Joint Research Center of Belgorod State National Research University “Technology and Materials” the activity of which was supported from the Ministry of Science and Higher Education of the Russian Federation within the framework of agreement no. 075-15-2021-690 (unique identifier for the project RF 2296.61321X0030).

CONFLICT OF INTEREST

The authors declare that they have no conflicts of interest.

REFERENCES

1. F. Abe, T. U. Kern, et al., *Creep-Resistant Steel* (Woodhead Publ., Cambridge, 2008).
2. R. O. Kaibyshev, V. N. Skorobogatykh, and I. A. Shchenkova, “New martensitic steels for thermal power plant: creep resistance,” *Phys. Met. Metallogr.* **109** (2), 186–201 (2010).
3. F. Abe, “Precipitate design for creep strengthening of 9% Cr tempered martensitic steel for ultra-supercritical power plants,” *Sci. Technol. Adv. Mater.* **9**, 013002 (2008).
4. F. Abe, T. Ohba, H. Miyazaki, Y. Toda, and M. Tabuchi, “Effect of W–Mo balance and boron content on creep rupture ductility of 9Cr steel,” *Mater. High Temp.* **36**, 368–378 (2019).
5. N. Dudova, R. Mishnev, and R. Kaibyshev, “Creep behavior of a 10% Cr high-resistant martensitic steel with low nitrogen and high boron contents at 650°C,” *Mater. Sci. Eng. A* **766**, 138353 (2019).
6. K. Maruyama, K. Savada, and J. Koike, “Strengthening mechanism of creep resistant tempered martensitic steel,” *ISIJ Int.* **41**, 641–653 (2001).
7. I. Nikitin, A. Fedoseeva, and R. Kaibyshev, “Strengthening mechanism of creep resistant 12% Cr–3% Co steel with low nitrogen and high boron contents,” *J. Mater. Sci.* **55**, 7530–7545 (2020).
8. F. Abe, “Progress in creep-resistant steels for high efficiency coal-fired power plants,” *J. Pres. Ves. Technol.* **138**, 040804 (2016).
9. H. K. Danielsen, “Review of Z phase precipitation in 9–12 wt % Cr steels,” *J. Mater. Sci. Technol.* **32**, 126–137 (2016).
10. K. Maruyama, N. Sekido, and K. Yoshimi, “Changes in strengthening mechanisms in creep of 9Cr–1.8W–0.5Mo–V–Nb steel tested over wide ranges of creep conditions,” *ISIJ Intern.* **190**, 1089–1094 (2021).
11. V. A. Dudko, A. N. Belyakov, V. N. Skorobogatykh, I. A. Shchenkova, and R. O. Kaibyshev, “Effect of austenitizing temperature on creep resistance of steel 10Kh9VMFBR,” *Metal Sci. Heat Treatment* **52**, 166–170 (2010).
12. F. Abe, “Effect of quenching, tempering, and cold rolling on creep deformation behavior of a tempered martensitic 9Cr–1W steel,” *Met. Mater. Trans. A* **34**, 913–925 (2003).

13. K. Kimura, N. Ohi, K. Shimazu, T. Matsuo, R. Tanaka, and M. Kikuchi, "Effect of prior austenite grain size on high temperature creep properties of Cr–Mo–V rotor steel," *Scr. Metall.* **21**, 19–22 (1987).
14. A. E. Fedoseeva, I. S. Nikitin, and R. O. Kaibyshev, "Effect of the quenching temperature on the creep Resistance of 9% Cr–1% W–1% Mo–V–Nb martensite steel," *Phys. Met. Metallogr.* **123** (1), 92–98 (2022).
15. A. E. Fedoseeva, I. S. Nikitin, N. Dudova, and R. O. Kaibyshev, "Superior creep resistance o a high-Cr steel with Re additives," *Mater. Lett.* **262**, 127183 (2020).
16. A. Zhilyaev, S. Sergeev, and T. Langdon, "Electron backscatter diffraction (EBSD) microstructure evolution in HPT copper annealed at a low temperature," *J. Mater. Res. Technol.* **3**, 338–343 (2014).
17. B. Wilshire and P. J. Scharring, "Prediction of long term creep data for forged 1Cr–1Mo–0.25V steel," *Mater. Sci. Technol.* **24** (1), 1–9 (2008).
18. F. J. Humphreys, M. Hatherly, et al., *Recrystallization and Related Annealing Phenomena* (Elsevier, 2012).
19. A. E. Fedoseeva, I. S. Nikitin, N. Dudova, and R. O. Kaibyshev, "Nucleation of W-rich carbides and Laves phase in a Re-containing 10% Cr steel during creep at 650°C," *Mater. Charact.* **169**, 110651 (2020).
20. V. M. Gundyrev, V. I. Zel'dovich, and V. M. Schastlivtsev, "Crystallographic analysis and the mechanism of martensitic transformation in Fe alloys," *Phys. Met. Metallogr.* **121** (11), 1045–1063 (2020).
21. V. V. Sagaradze, T. N. Kocheikova, N. V. Kataeva, K. A. Kozlov, V. A. Zavalishin, N. F. Vil'danova, V. S. Ageev, M. V. Leont'eva-Smirnova, and A. A. Nikitina, "Structure and creep of Russian reactor steel with a bcc structure," *Phys. Met. Metallogr.* **118** (5), 494–506 (2017).
22. A. Fedoseeva, I. Nikitin, E. Tkachev, R. Mishnev, N. Dudova, and R. O. Kaibyshev, "Effect of alloying on the nucleation and growth of Laves phase in the 9–10% Cr–3% Co martensitic steel during creep," *Metals* **11**, 60 (2021).
23. M. Lifshitz and V. V. Slyozov, "The kinetics of precipitation from super-saturated solid solutions," *J. Phys. Chem. Sol.* **19**, 35–50 (1961).
24. R. Wagner and R. Kampmann, in *Homogeneous Second Phase Precipitation* (Wiley, New York, 1991), pp. 213–303.
25. F. Abe, "Effect of fine precipitation and subsequent coarsening of Fe₂W Laves phase on the crepe formation behavior of tempered martensitic 9Cr–W steels," *Met. Mater Trns. A* **36**, 321–332 (2005).
26. F. Abe and S. Nakazawa, "The effect of tungsten on creep," *Met. Trans. A* **23**, 3025–3034 (1992).

Translated by Yu. Ryzhkov